

APPLICATION OF THE SHALLOW WATER EQUATIONS TO REAL FLOODING CASE

H. Ali¹, P-Y. Lagrée², and J-M. Fullana²

¹AXA Global P&C, 75008 Paris, France
e-mail: hani.ali@axa.com

² Institut Jean le Rond d'Alembert, CNRS & UPMC Université Paris 06, UMR 7190, 75005 Paris, France
e-mail: {pierre-yves.lagree,jose.fullana}@upmc.fr

Keywords: Shallow-Water equations, Computational Methods, Engineering Sciences.

Abstract. *In this paper, we solve and validate the Shallow Water equations with a well-balanced finite volume method and semi-implicit treatment of the friction term. The method is validated by simulating the Seine river flooding (France 1910), which is served as a benchmark. The method is implemented in the open source software Basilisk which is freely available at <http://www.basilisk.fr>. Furthermore, we compare the obtained result with Basilisk to a simple propagation model developed by the actuary team at AXA Global P&C.*

1 INTRODUCTION

The Shallow Water equations (or Saint-Venant Equations) are commonly used to represent the flow of water under the assumption that the characteristic vertical length scale of the flow is very small with respect to the characteristic horizontal length scale. These equations can be obtained by depth averaging the incompressible three dimensional Navier-Stokes equations under the previous assumption in the vertical direction. This results in neglecting any acceleration in the direction of the gravity, which gives rise to a hydrostatic pressure distribution.

The numerical resolution of the Shallow Water equations is a good tool to predict flow properties in various situation such as Dam Breaks [15, 5], Tsunami propagation [10], Rivers flows [2] and flooding [3, 6], among others as there is a huge literature on the Shallow Water equations.

The Shallow Water equations are given by the following system:

$$\begin{aligned} \partial_t h + \partial_x(hu) + \partial_y(hv) &= 0, \\ \partial_t(hu) + \partial_x(hu^2 + gh^2/2) + \partial_y(huv) &= gh(S_{0_x} - S_{f_x}), \\ \partial_t(hv) + \partial_x(huv) + \partial_y(hv^2 + gh^2/2) &= gh(S_{0_y} - S_{f_y}). \end{aligned} \quad (1)$$

Here:

- $u(x, y, t)$ and $v(x, y, t)$ are the scalar components in the horizontal direction (x, y) of the depth-averaged velocity for a given time $t > 0$,
- $h(x, y, t)$ is the local water depth,
- $g = 9.81m/s^2$ is the gravity constant,
- $\mathbf{S}_0 = (S_{0_x}, S_{0_y}) = (-\partial_x z(x, y), -\partial_y z(x, y))$ is the linearized bed slope, where $z(x, y)$ is the topography,
- and $\mathbf{S}_f = (S_{f_x}, S_{f_y}) = (n^2 \frac{\sqrt{u^2+v^2}}{h^{4/3}} u, n^2 \frac{\sqrt{u^2+v^2}}{h^{4/3}} v)$, is the friction force, where n is the Manning's coefficient which depends on the considered type of soil (see [4]).

In this paper we aim to study an application of the Shallow Water equations to a real life flooding case. The application consists in simulating the flooding of the Seine river in Paris which occurred in January 1910. Predicting this flooding represents a challenge for public policy. In fact, the damage that could be caused by a potential flood having the same level as in 1910 is considerable, especially in Paris where the main activity pool of the French economy is concentrated.

The first difficulty before running the simulation with the SWE is the choice of the numerical scheme. Referring to the work of [1] see also [6], we consider a hydrostatic reconstruction scheme coupled with a semi implicit treatment of the friction term to avoid spurious flows due to topography. Second, we have to consider the appropriate topography that is relevant to the physical one. Given that we are limited by the computer power and by the availability of such topography, we choose to use a free available topography from the National Institute of Geographic and Forest Information (IGN) where a mesh of 75 m is used. First, we will use the topography in its original form. Second, we will modify the topography in order to take into account the so called barriers at the main bed of the river. We will use in all these simulations the open source code Basilisk which is a C code based on a finite volume method

with a structured mesh. This code uses also a quadtrees mesh to allow efficient adaptive grid refinement. Methods based on quadtrees mesh have been successfully used to compute adaptive solutions of many problems such as the 2D and the 3D Navier-Stokes equations [13, 12] or Shallow Water equations [14].

The rest of this paper is organized as follows: In section 2, we set up the formulation of the model equations and recall the numerical scheme. In section 3, we reproduce the 1910 flooding in Paris by using the historical registration of the water depth. We superimpose some obtained footprints with some maps from [8] in order to visualize clearly the inundated regions. Furthermore, we compare our result against the result that is furnished by the Regional and Interdepartmental Directorate of Environment and Energy (DRIEE) in order to validate our method. In section 4, we study the sensitivity of the model with respect to the Manning's coefficient. In section 5, we compare the result furnished by the resolution of the SWE with the result obtained by a simple propagation model developed by the actuary team at AXA Global P&C. Section 6 contains the conclusion of this paper.

2 Numerical method

2.1 General form

The system 1 can be written in the conservative form as

$$\partial_t \mathbf{U} + \nabla (\mathbf{F}, \mathbf{G}) = \mathbf{R}, \quad (2)$$

where

$$\begin{aligned} \mathbf{U} &= (h, hu, hv), \quad \mathbf{F} = (hu, hu^2 + gh^2/2, huv), \\ \mathbf{G} &= (hv, huv, hv^2 + gh^2/2), \\ \text{and } \mathbf{R} &= (0, gh(S_{0_x} - S_{f_x}), gh(S_{0_y} - S_{f_y})). \end{aligned} \quad (3)$$

Here, \mathbf{U} is the vector of conserved variables, \mathbf{F} and \mathbf{G} are the flux functions, and \mathbf{R} stands for the sources which are formed from the bed slope $gh(\mathbf{S}_0)$ term and the friction term $gh(\mathbf{S}_f)$. We note that for $h > 0$ the above system is strictly hyperbolic.

As the 2D case can be treated by a complete analogy with the 1D case, for seek to simplicity, we will consider only the 1D case. The two-dimensional system (2) rewrite

$$\partial_t \mathbf{U} + \partial_x \mathbf{F} = \mathbf{R}. \quad (4)$$

Hereafter,

$$\mathbf{U} = (h, hu), \quad \mathbf{F} = (hu, hu^2 + gh^2/2), \quad \text{and } \mathbf{R} = (0, gh(S_{0_x} - S_{f_x})). \quad (5)$$

We split in two problems, first an inviscid one, second a purely viscous one.

2.2 Inviscid part treatment

Following [1], we use the hydrostatic reconstruction scheme to the problem (4), without the friction term, which is given by

$$\mathbf{U}_i^* = \mathbf{U}_i^n - \frac{\Delta t}{\Delta x} (\mathbf{F}_{i+1/2}^n - \mathbf{F}_{i-1/2}^n) + \frac{\Delta t}{\Delta x} \mathbf{S}_{0_i}^n, \quad (6)$$

where

$$\mathbf{F}_{i+1/2}^n = \mathcal{F}(\mathbf{U}_{i+1/2,L}^n, \mathbf{U}_{i+1/2,R}^n), \quad \mathbf{F}_{i-1/2}^n = \mathcal{F}(\mathbf{U}_{i-1/2,L}^n, \mathbf{U}_{i-1/2,R}^n), \quad (7)$$

and

$$\mathbf{S}_i^n = (0, g(h_{i+1/2,L}^n)^2/2 - g(h_{i-1/2,R}^n)^2/2). \quad (8)$$

Here \mathcal{F} stands to the numerical flux which is defined in the next section and the values of $\mathbf{U}_{i+1/2,L}^n$ and $\mathbf{U}_{i+1/2,R}^n$ are obtained by applying once again the hydrostatic reconstruction.

$$\mathbf{U}_{i+1/2,L}^n = (h_{i+1/2,L}^n, h_{i+1/2,L}^n u_i^n), \quad \mathbf{U}_{i+1/2,R}^n = (h_{i+1/2,R}^n, h_{i+1/2,R}^n u_{i+1}^n) \quad (9)$$

where

$$\begin{aligned} h_{i+1/2,L}^n &= \max(0, h_i^n + z_i^n - \max(z_i^n, z_{i+1}^n)), \\ h_{i+1/2,R}^n &= \max(0, h_{i+1}^n + z_{i+1}^n - \max(z_i^n, z_{i+1}^n)). \end{aligned} \quad (10)$$

We note that this scheme is designed to capture the dry regions where $h = 0$ and to ensure the non-negativity of the water weight, we refer the reader to [1] for more details.

2.3 Numerical flux

In Basilisk many consistent flows were implemented for the homogeneous part of the system 2, for example the Harten Lax Van Leer (HLL) flux, the Kurganov flux and the one obtained by the kinetic method. In this work we used the Kurganov flux. The Kurganov flux [11] is based on a central-upwind scheme which does not require exact or approximate Riemann solvers and a characteristic analysis that upwind Godunov-type methods require. Furthermore, they admit a less numerical dissipation than the other numerical flux.

The application of this scheme gives the following expression for the numerical flux:

$$\begin{aligned} \mathcal{F}(\mathbf{U}_{i+1/2,L}^n, \mathbf{U}_{i+1/2,R}^n) &= \frac{a_{i+1/2,R} \mathbf{F}(\mathbf{U}_{i+1/2,L}^n) - a_{i+1/2,L} \mathbf{F}(\mathbf{U}_{i+1/2,R}^n)}{a_{i+1/2,R} - a_{i+1/2,L}} \\ &+ \frac{a_{i+1/2,R} a_{i+1/2,L}}{a_{i+1/2,R} - a_{i+1/2,L}} (\mathbf{U}_{i+1/2,L}^n - \mathbf{U}_{i+1/2,R}^n), \end{aligned} \quad (11)$$

where

$$\begin{aligned} a_{i+1/2,R} &= \max(0, u_{i+1/2,R}^n + \sqrt{gh_{i+1/2,R}^n}, u_{i+1/2,L}^n + \sqrt{gh_{i+1/2,L}^n}), \\ a_{i+1/2,L} &= \min(0, u_{i+1/2,R}^n - \sqrt{gh_{i+1/2,R}^n}, u_{i+1/2,L}^n - \sqrt{gh_{i+1/2,L}^n}). \end{aligned} \quad (12)$$

The above scheme is stable under the following CFL condition on the time step Δt :

$$\Delta t \leq CFL \frac{\Delta x}{\max(a_{i+1/2,R}, -a_{i+1/2,L})}, \quad (13)$$

where $CFL < 1$ is the Courant number and Δx is the space step.

2.4 Friction term treatment

The fractional-step method is a standard way to deal with the friction term. The complete solution of problem (2) is obtained by first solving the equations without the friction term as in section 2.1 to obtain an intermediate solution \mathbf{U}^* . The following problem is then solved using \mathbf{U}^* to find the complete solution \mathbf{U}^{n+1} :

$$\partial_t \mathbf{U} = \mathbf{S}_f. \quad (14)$$

Thus, we obtain the following semi-implicit scheme for the friction term

$$h^{n+1} = h^* \quad \text{and} \quad u^{n+1} = \frac{u^*}{1 + g\Delta t n^2 \frac{|u^n|}{(h^{n+1})^{4/3}}}. \quad (15)$$

We note that this semi-implicit scheme preserves the steady state at rest and also the stability under the CFL condition.

3 Numerical simulation: application to Seine inundation

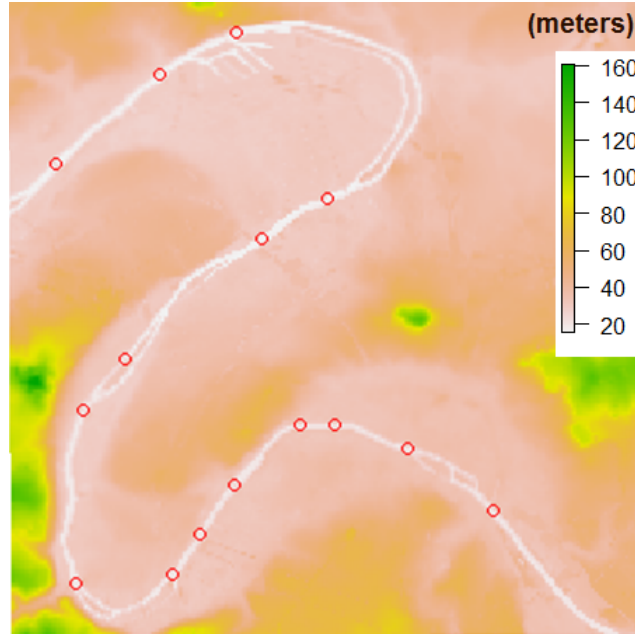


Figure 1: Topography generated from the IGN data showing the domain of the study with 75 m mesh resolution, $23.6 \text{ m} \leq z \leq 161 \text{ m}$. Locations of different gauges are given.

The Seine river in Paris is our case study. Figure 1 represents the topography of the river in the landscape: the upstream end is located near Austerlitz train station and the downstream end is located near Chatou train station. The domain area is about 225 km^2 .

We will distinguish between two cases: First, we run the simulation by using the topography that is furnished by the IGN ([9]). Second, we modify the topography in order to take into account the barriers along the river which are constructed to prevent flooding (see figure 2).

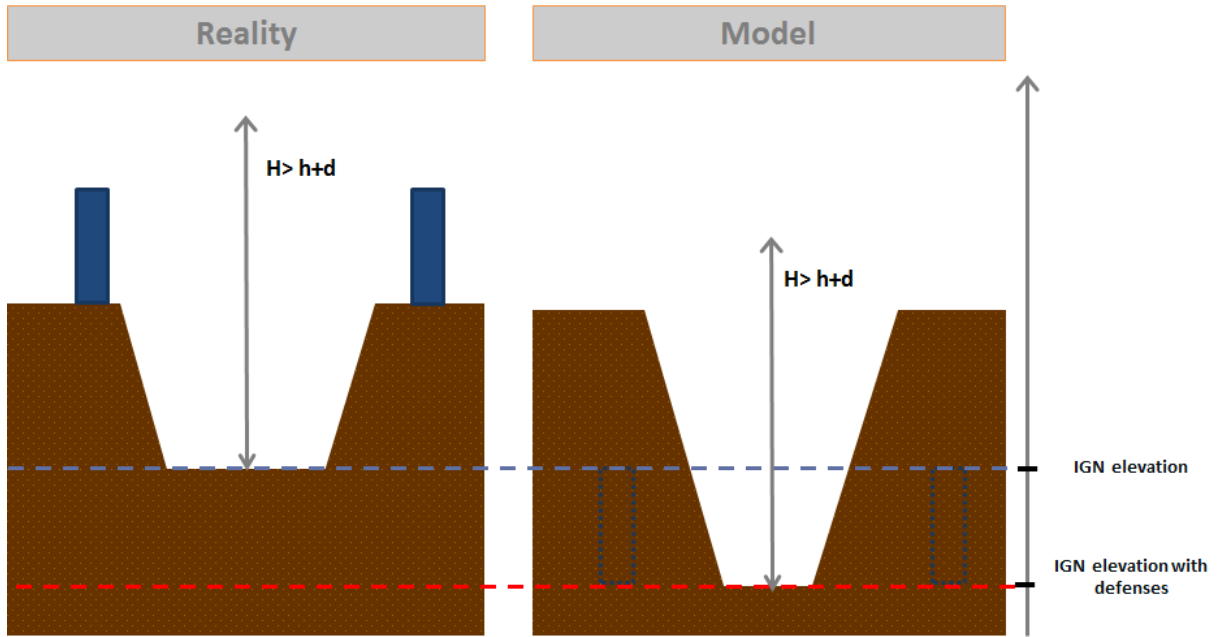


Figure 2: Figure showing the modified topography

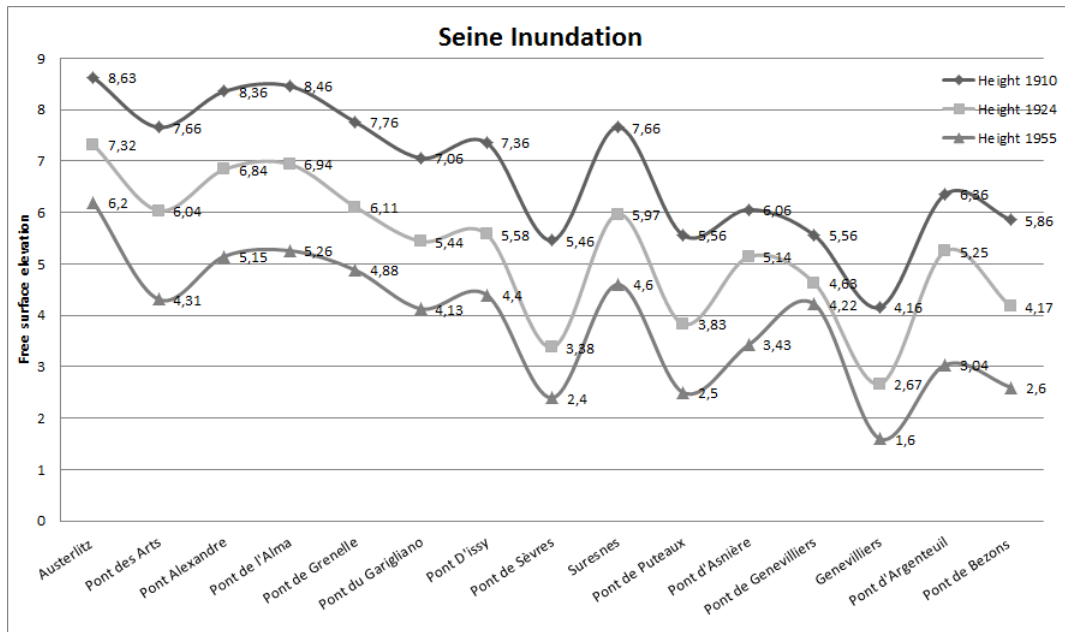


Figure 3: Free elevation final height at several places in Paris, computed values

3.1 Numerical resolution and the raw IGN data

The numerical solution has been computed by using the SWE described in section 2, where the topography is given by the IGN (see figure 1). The Manning's coefficient n is set to $0.01 \text{ s/m}^{\frac{1}{3}}$ for two reasons: First, in order to accelerate the propagation of the water. Second, in order to represent the minor and major bed of the Seine river at Paris as a firm soil.



Figure 4: A figure generated from simulation at $t = 120000s$ showing the inundated area in 1910

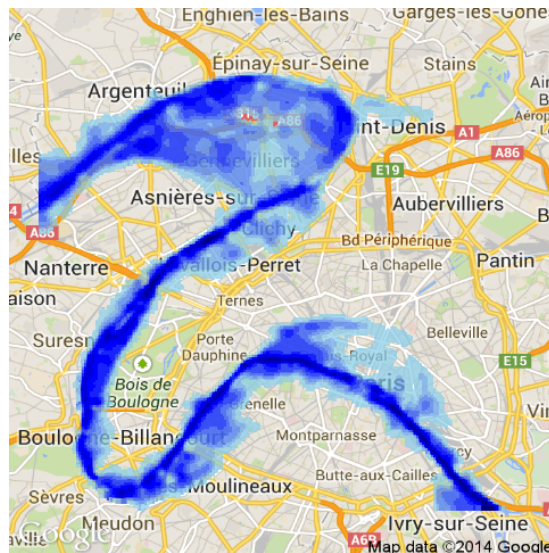


Figure 5: A figure generated from simulation at $t = 120000s$ showing the inundated area in 1924

Figure 3 shows the evolution of the water depth in meters between Austerlitz and the Bridge of Bezons. This figure gives the level of the free surface, i.e. the depth of the water, at each station.

We took as a reference the historical depth of the water in Austerlitz in 1910, 1924 and 1982. Within the used IGN topography, the altitude of Austerlitz is about 27 m from the zero level which is the NGF69 level. Thus, we take into account this information in order to reproduce the historical events. The numerical results at the final stage after 12h of propagation is given in figures 4, 5 and 6. These figures allow us to determine the inundated regions in Paris in 1910, 1924 and 1982.



Figure 6: A figure generated from simulation at $t = 120000s$ showing the inundated area in 1982

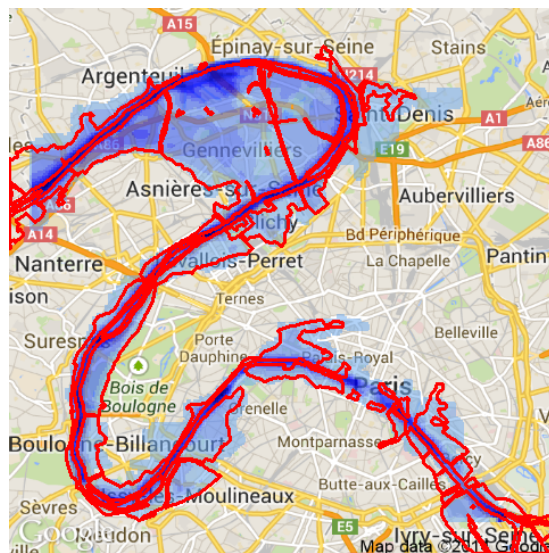


Figure 7: A figure generated from simulation at $t = 120000s$ showing a comparison between our simulation (blue) and the result of the DRIEE (red).

3.2 Simulation with defenses

Next, we will modify the topography in order to take into account the barriers along the river. These barriers reach the value of 7m in Austerlitz. Here, we compare our simulation with the modified topography that we call simulation with defenses against the result that are furnished by the DRIEE [7]. Figure 7 shows that our result is consistent with the DRIEE result. In order to calculate the prediction rate we calculate the ratio between the inundated area given by our simulation and the inundated area given by the DRIEE. We deduce that our result is similar to the result of the DRIEE with a prediction rate of 90 percent. The regions that are potentially inundated can be detected from this figure.

4 Sensitivity to Manning's coefficient

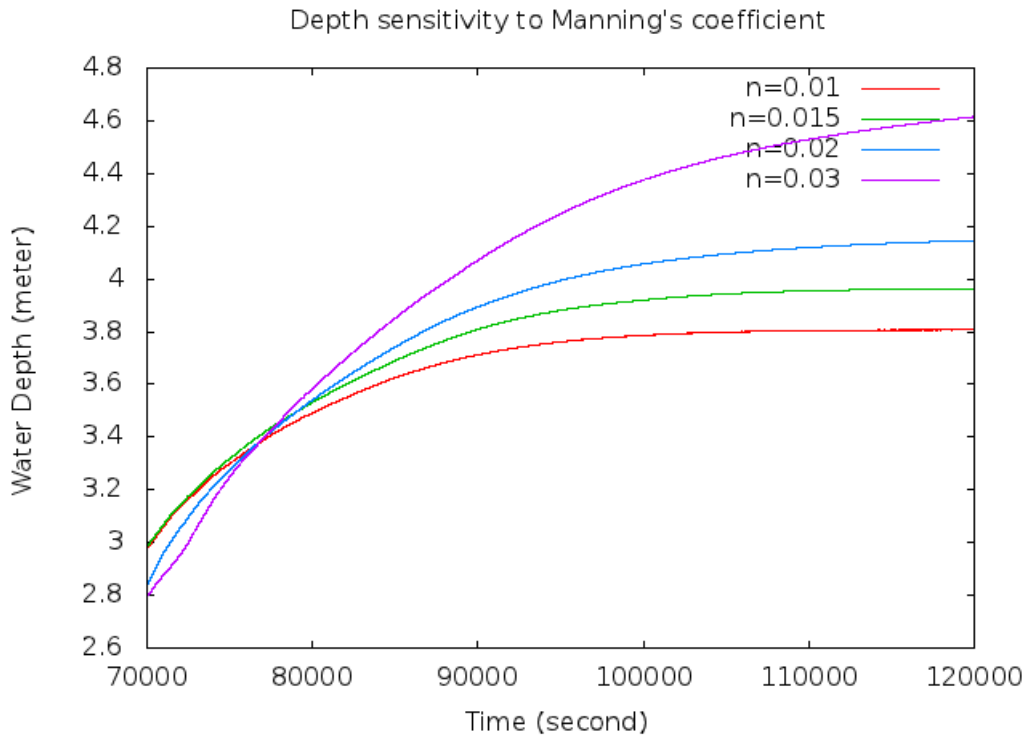


Figure 8: Variations of the water depth with respect to the manning's coefficient n . The gauge is located near Issy bridge in Paris

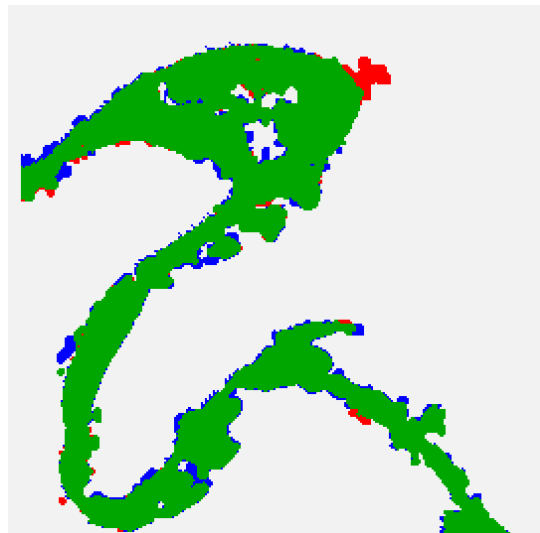


Figure 9: A figure generated from simulation at $t = 120000s$ showing a comparison between the inundated area in 1982 with $n = 0.01$ (blue) and with $n = 0.015$ (red) and their intersection (green)

The Manning's coefficient n is the most important parameter that should be determined for hydrodynamics models. In fact, selecting the value of n means to estimate the flow resistance

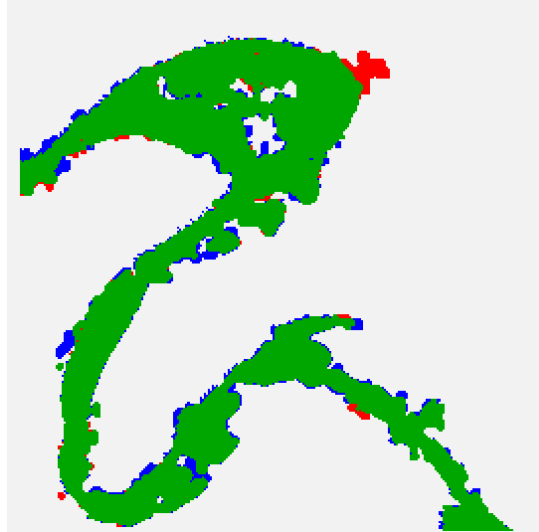


Figure 10: A figure generated from simulation at $t = 120000s$ showing a comparison between the inundated area in 1982 with $n = 0.01$ (blue) and with $n = 0.02$ (red) and their intersection (green)

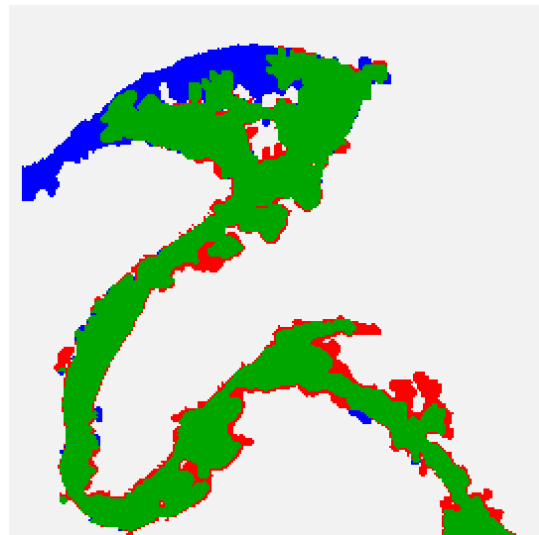


Figure 11: A figure generated from simulation at $t = 120000s$ showing a comparison between the inundated area in 1982 with $n = 0.01$ (blue) and with $n = 0.03$ (red) and their intersection (green)

to the movement. Moreover, this coefficient greatly impacts the flow speed, which then impacts the depth and the flood extent. In order to test the sensitivity of the model with respect to the Manning's coefficient, we run the simulation for four values of n 0.01, 0.015, 0.02, and 0.03. These values seem reasonable for a river channel with a firm soil bed and no vegetation.

Figure 8 shows that when n is bigger than 0.01 the flow is slower and the water can be more accumulated. A comparison between the footprint of the 1982 flood in Paris with $n = 0.01$ and $n = 0.015$, $n = 0.02$, and $n = 0.03$ respectively at the same time are given in figures 9, 10 and 10. These figures show that the new inundated region will be bigger than that given before for $n = 0.01$. However, the water propagation will be slower than that given before for $n = 0.01$ as we see that at the final time of our simulations the water does not attain yet the downstream

end of the domain for $n = 0.02$ and $n = 0.03$.

5 Comparaison between a simple propagation model and the SWE

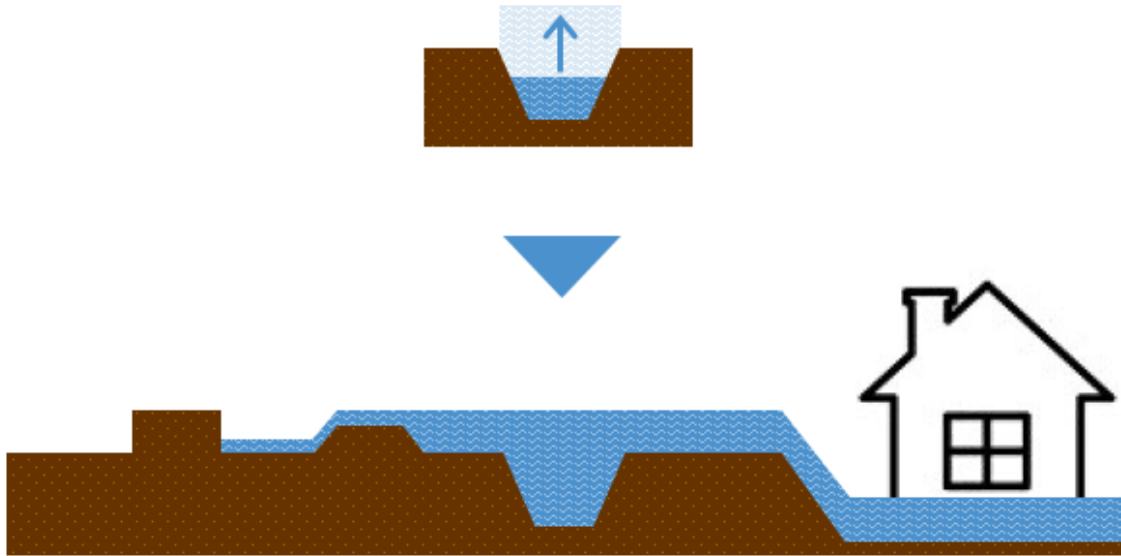


Figure 12: Figure showing the propagation algorithm with R which is developed at AXA Global P&C

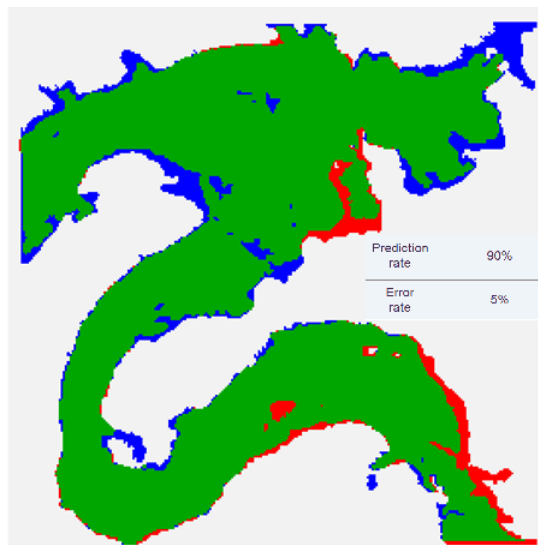


Figure 13: A figure generated from simulation showing a comparison between a simple filling method with Basilisk (blue) and the simulation with the simple propagation algorithm (red)

In this section, we give a comparative study between the model based on the resolution of the SWE (described above) and a propagation model which is developed by the actuary team at AXA Global P&C. This propagation model is simpler than that based on the resolution of

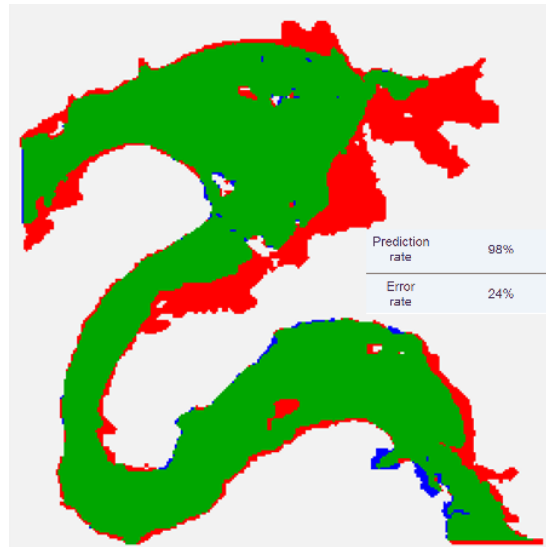


Figure 14: A figure generated from simulation showing a comparison between the inundated area in 1910 obtained with Basilisk at $t = 120000s$ (blue) and the simulation obtained with the propagation algorithm with non-uniform initial height (red) and their intersection (green)

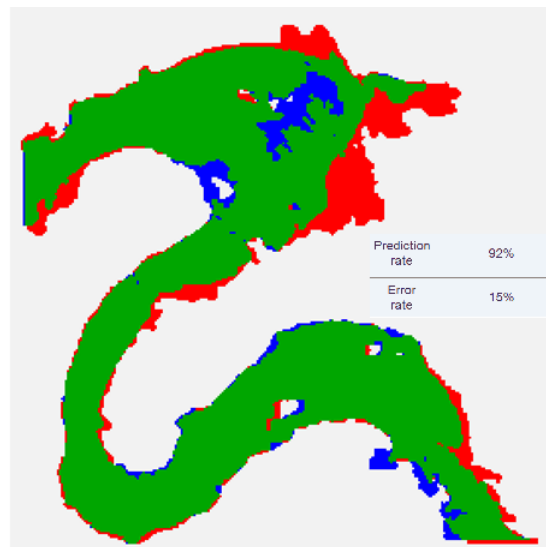


Figure 15: A figure generated from simulation showing a comparison between the inundated area in 1910 obtained with Basilisk at $t = 120000s$ (blue) and the simulation obtained with the propagation algorithm with non-uniform initial height and a dissipative term (red) and their intersection (green)

the SWE. It allows us to obtain footprint of the inundation. This model is programmed in R language and verifies the following properties (see figure 12):

- A cell is only flooded by one of its 8 direct neighbors
- The water level of a flooded cell is the maximum of its flooded neighbors
- The water depth of a cell cannot exceed the largest depth of its neighbors

In order to evaluate the performance of this simple propagation model, we will compare between the footprint obtained by this model for Paris flooding in 1910 and the footprint obtained

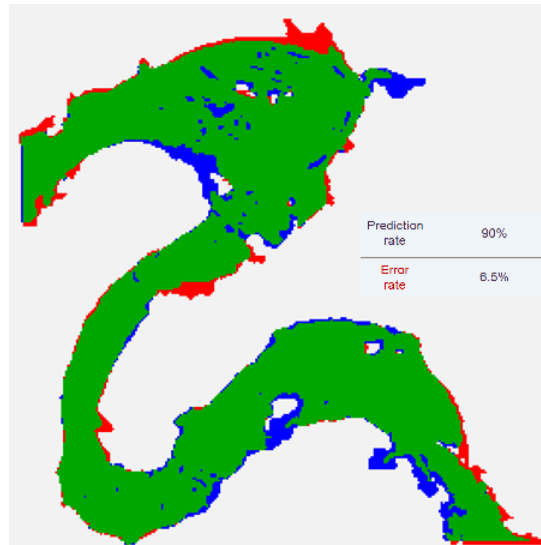


Figure 16: A figure generated from simulation showing a comparison between the inundated area in 1910 obtained with Basilisk at $t = 120000s$ (blue) and the simulation obtained with the propagation algorithm with non-uniform initial height and an interpolated topography (red) and their intersection (green)

above using the SWE. In both models, we use the IGN Digital elevation data with 75 m resolution. Figure 13 shows a comparison between the result of the flooding scenario with Basilisk, by filling in all the regions with a depth less than 35 m, and the result of the simple propagation algorithm. It can be seen that both models match well. The inundated region in figure 13 is clearly bigger than the one obtained in figure 4 with the hydrodynamic model. We deduce from this visual index that the simple model needs to be calibrated with respect to the hydrodynamic model in order to obtain a better approximation of the inundated region. For this reason, we consider first the simple propagation algorithm with a non-uniform height along the major bed and second by adding a dissipative term in the algorithm. These both modifications allow us to reduce the inundated region and thus ameliorate the error ratio (see figures 14 and 15), i.e. the over detected area, defined as the ratio of the area obtained with the simple algorithm which does not belong to the intersection area (the red area), and the area obtained with the same algorithm (error ratio = $\frac{\text{red area}}{\text{red area} + \text{green area}}$). Moreover, in both cases, the prediction ratio is greater than 90%, where the prediction ratio is defined as the ratio of the intersection area and the area obtained with the SWE model (prediction ratio = $\frac{\text{green area}}{\text{blue area} + \text{green area}}$).

Another way to calibrate the simple model written in R with respect to the simulation result obtained with Basilisk is to interpolate manually in R the furnished topography from IGN. In fact, Basilisk interpolates automatically the topography whenever the gradient of the height h is greater than 10 cm. Thus, we get in the final stage of the simulation with Basilisk an interpolated topography with approximately 25 m grid resolution. Figure 16 shows that the calibrated algorithm with the interpolated topography with (25 m grid resolution) approximates well the hydrodynamic model. Thus, a better resolution of the digital elevation model has a profound impact on the accuracy of the footprint extent.

6 Conclusion

From this case study, we can conclude that both models, the hydrodynamic model, based on the SWE, and the calibrated simple model, are able to simulate the inundated extent region of

Paris 1910 flood with a certain accuracy level. The hydrodynamic 2D model gave the best overall performances and a more precise information about the depth, the extent and the velocity of the flow. Basilisk code uses digital elevation models and generates the topography required by the hydrodynamic model. The mathematical model utilizes the SWE written in their conservative form without any simplification. Furthermore, the numerical method used is stable, which makes the Basilisk code suitable for practical applications.

However, the major obstacle of the simulation concerns the long runtime of the hydrodynamic model which is about 3 hours. This long runtime is needed to better calibrate the model with respect to the Manning coefficient. This is still the major disadvantage of the hydrodynamic model even with the adaptive meshes.

Furthermore, the Basilisk code should be tested with a better resolution grid for the DEM. Using a better resolution grid for the DEM has also the disadvantage of the calculation time which becomes again longer. Thus, a balance must be found between the available DEM's with different resolution, the runtime of the simulation, and the method accuracy.

The calibrated simple model worked well in the case of Paris flooding without defenses. Thus, one can use the calibrated simple model when we do not need a lot of precision. Further test cases should be undertaken to validate the general applicability of this conclusion. In particular, we need first to test this model to simulate Paris 1910 flood scenario with defenses and also simulate the flooding of other regions of the river where the morphology of the floodplain is different.

REFERENCES

- [1] E., Audusse, F., Bouchut ,M.-o., Bristeau, R., Klein, B., Perthame, A fast and stable well-balanced scheme with hydrostatic reconstruction for shallow water flows, *SIAM J. Sci. Comp.*, **25**, 2050–2065, 2004.
- [2] J., Burguete, P., Garcia-Navarro, Implicit schemes with large time step for non-linear equations : application to river flow hydraulics, *International Journal for Numerical Methods in Fluids*, **46**, 607–636, 2004.
- [3] V., Caleffi, A. , Valiani, A., Zanni, Finite volume method for simulating extreme flood events in natural channels, *Journal of Hydraulic Research*, **41**, 167–177, 2003.
- [4] V. T., Chow, *Open-Channel Hydraulics*, N. York, Ed. McGraw-Hill, 1959.
- [5] S., Cordier, H., Coullon, O., Delestre, C., Lauerre, M.H. Le D., Pierre, G. Sadaka, Fullswofparal: Comparison of two parallelization strategies mpi and skelgis on a software designed for hydrology applications, *ESAIM Proceedings*, **43**, 59–79, 2013.
- [6] O., Delestre, S., Cordier, F., James, F., Darboux, Simulation of rain-water overland-flow, *Proceeding of symposia in Applied Mathematics*, **67**, 537–546, 2009.
- [7] DRIEE, *Les scenarios de crue en région île-de-france*, 1–22, 2012, available at <http://www.driee.ille-de-france.developpement-durable.gouv.fr/scenarios-de-crue-a1075.html>.
- [8] GoogleMaps, 2014, available at <https://maps.google.fr>.
- [9] IGN, Bd alti, 2014, available at <http://professionnels.ign.fr/bdalti>.

- [10] D.-H., Kim, Y.-S., Cho, Y.-K., Yi, Propagation and run-up of near shore tsunamis with HLLC approximate riemann solver, *Ocean Engineering*, **34**, 1164–1173, 2007.
- [11] A., Kurganov, D., Levy, Central-upwind schemes for the saint-venant system, *Mathematical Modeling and Numerical Analysis*, **36**, 397–425, 2002.
- [12] S., Popinet, An accurate adaptive solver for surface-tension-driven interfacial flows, *J Comput Phys*, **228**, 5838–5866, 2003.
- [13] S., Popinet, Gerris: a tree-based adaptive solver for the incompressible Euler equations in complex geometries, *J Comput Phys*, **2**, 572–600, 2003.
- [14] S., Popinet, G., Rickard, A tree-based solver for adaptive ocean modelling, *Ocean Model*, **16**, 224–249, 2007.
- [15] A., Valiani, , V., Caleffi, A., Zanni, Case study : Malpasset dam-break simulation using a two-dimensional finite volume methods, *Journal of Hydraulic Engineering*, **128**, 440–472, 2002.